



CHALMERS

Chalmers Publication Library

Antenna-integrated 0.6 THz FET direct detectors based on CVD graphene

This document has been downloaded from Chalmers Publication Library (CPL). It is the author's version of a work that was accepted for publication in:

Nano letters (ISSN: 1530-6984)

Citation for the published paper:

Zak, A. ; Andersson, M. ; Bauer, M. et al. (2014) "Antenna-integrated 0.6 THz FET direct detectors based on CVD graphene". Nano letters, vol. 14(10), pp. 5834-5838.

<http://dx.doi.org/10.1021/nl5027309>

Downloaded from: <http://publications.lib.chalmers.se/publication/202575>

Notice: Changes introduced as a result of publishing processes such as copy-editing and formatting may not be reflected in this document. For a definitive version of this work, please refer to the published source. Please note that access to the published version might require a subscription.

Chalmers Publication Library (CPL) offers the possibility of retrieving research publications produced at Chalmers University of Technology. It covers all types of publications: articles, dissertations, licentiate theses, masters theses, conference papers, reports etc. Since 2006 it is the official tool for Chalmers official publication statistics. To ensure that Chalmers research results are disseminated as widely as possible, an Open Access Policy has been adopted. The CPL service is administrated and maintained by Chalmers Library.

(article starts on next page)

Antenna-integrated 0.6 THz FET direct detectors based on CVD graphene

Michael A. Andersson†, Audrey Zak*†, Maris Bauer*‡, Jonas Matukas◇, Alvydas Lisauskas‡◇,
Hartmut G. Roskos‡, Jan Stake†.*

AUTHOR ADDRESS † Department of Microtechnology and Nanoscience, Chalmers University of Technology, SE-412 96 Gothenburg, Sweden, ‡ Physikalisches Institut, Johann Wolfgang Goethe-Universität, DE-60438 Frankfurt am Main, Germany, ◇ Radiophysics Department, Vilnius University, LT-10222 Vilnius, Lithuania.

KEYWORDS Graphene field effect transistors, direct terahertz detection, CVD graphene, antenna-integrated detectors, distributed resistive self-mixing.

ABSTRACT We present terahertz (THz) detectors based on top-gated graphene field effect transistors (GFETs) with integrated split-bow-tie antennas. The GFETs were fabricated using graphene grown by chemical vapor deposition (CVD). The THz detectors are capable of room-temperature rectification of a 0.6 THz signal and achieve a maximum optical responsivity better than 14 V/W and minimum optical noise-equivalent power (NEP) of 515 pW/Hz^{0.5}. Our results are a significant improvement over previous work on graphene direct detectors and are comparable to other established direct detector technologies. This is the first time room-

temperature direct detection has been demonstrated using CVD graphene, which introduces the potential for scalable, wafer-level production of graphene detectors.

Interest in terahertz (THz) technology has recently been on the rise due to the potential to use terahertz radiation for a variety of applications including security imaging,¹ spectroscopy,² biomedical imaging,³ and even anthropology.⁴ This necessitates the development of reliable, room-temperature terahertz sources and detectors.⁵ In this context, field effect transistors (FETs) have shown their potential as sensitive THz detectors realized with various traditional semiconductor materials.⁶⁻¹⁰ In an effort to close the so-called *terahertz gap* (loosely defined as 0.3-10 THz) a focus is on high-mobility materials, and due to its high room-temperature mobility (up to 10,000 cm²/Vs on SiO₂) and high carrier saturation velocity,^{11,12} graphene has recently attracted interest as a potential material for high-frequency applications.^{13,14} Theoretical analysis of graphene confirms its potential for use as a THz FET detector.^{15,16} Successful operation of graphene field-effect transistors (GFETs) has been demonstrated at radio frequencies.¹⁷⁻²⁰ In the THz range, room-temperature detection with GFETs has been reported up to 3.11 THz.²¹⁻²³ Thus far, even the best graphene-based FET THz detectors have had noise-equivalent powers (NEPs) close to two orders of magnitude higher than those demonstrated in other material systems such as Si MOSFETs (>17 pW/Hz^{0.5})^{7,8} and GaN high-electron mobility transistors (40 pW/Hz^{0.5}),⁹ or than the NEPs of other detector technologies like YBCO bolometers (200 pW/Hz^{0.5}),²⁴ and zero-bias Schottky diode detectors (<20 pW/Hz^{0.5}).²⁵

Detection of THz radiation using field-effect transistors (FETs) can be explained by distributed resistive self-mixing of the incident THz signal in the FET channel.^{26,27} When the incident

radiation is fed to the drain and gate terminals of the transistor, the result is a drain-source current generated by the self-mixing of induced charge density oscillations (plasma waves) launched into the channel. At high frequencies, this principle of THz rectification in FETs can be described by hydrodynamic plasma wave models.^{26,28} If the damping of the plasma waves inside the channel is small and the channel is short, conditions can be fulfilled for enhanced resonant detection.^{15,26} Graphene is a promising candidate for such conditions because its high mobility should translate into a long carrier scattering time and therefore less damping of the plasma waves.

In this Letter, we present THz detection measurements with an antenna-integrated GFET detector fabricated using graphene grown by chemical vapor deposition (CVD). Figure 1(a) shows an SEM image of the fabricated device with the split bow-tie antenna structure, where the antenna bows act as the GFET electrodes as labeled. A schematic representation of the actual GFET including the device dimensions is depicted in Figure 1(b). The detectors were fabricated using single-layer graphene on Si/SiO₂ substrates (high-resistivity silicon with 300 nm SiO₂) prepared by CVD growth and transfer. Graphene was grown on a copper foil catalyst following the recipe of Sun and co-workers²⁹ and then transferred from the Cu foil to a 10 mm x 10 mm Si/SiO₂ substrate using a frame-assisted bubbling transfer process³⁰ and was verified to be single layer using optical microscopy and Raman spectroscopy. The source and drain contacts were patterned with electron beam lithography followed by evaporation and lift-off of a Ti/Pd/Au metal stack with thickness 1/15/300 nm. Graphene outside the channel area was etched and a 17-nm-Al₂O₃ gate oxide was deposited³¹ before a gold top-gate was patterned with electron beam lithography. For rectification by plasma wave mixing to be effective, asymmetric coupling

conditions to the transistor's contacts must be ensured. This was achieved by using a split bow-tie antenna, inducing capacitive coupling between the drain and gate terminals.

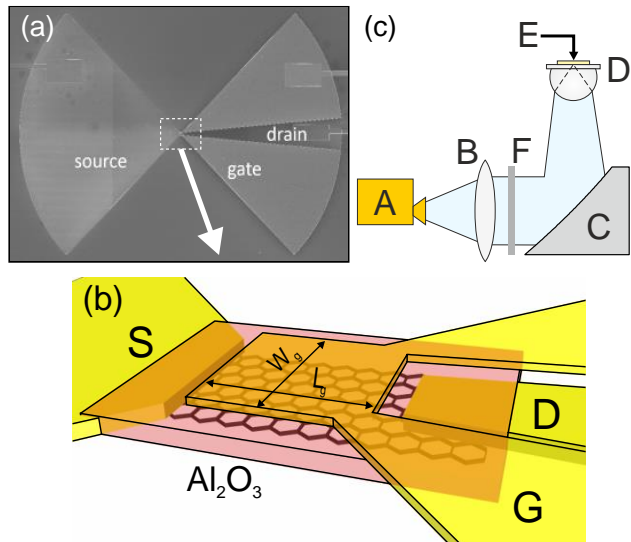


Figure 1. (a) SEM image of the split bow-tie integrated GFET detector with source (S), drain (D) and gate (G) contacts labeled. (b) Schematic of the GFET (rectangular area in (a), not to scale) with dimensions $W_g = 2 \mu\text{m}$, $L_g = 2.5 \mu\text{m}$ and S-D, D-G separation of 100 nm. (c) Measurement setup. The 0.6 THz source (A) is collimated by a PTFE lens (B), and focused onto the detector (E) by an off-axis paraboloidal mirror (C) and a hyper-hemispherical silicon lens (D). The beam power was measured after the lens with a Thomas Keating power meter (F). The sample was illuminated through the Si/SiO₂ substrate.

The resistance of the CVD GFET detector is shown in Figure 2(a). A known issue with GFETs is their hysteretic behavior depending on voltage sweep direction.³² To mitigate this effect, all data shown are measured with a negative-to-positive gate-voltage sweep. The resistance was obtained in two ways, first, from a direct current IV measurement and second, as the ratio of the rectified voltage and current responses ΔU and ΔI , respectively, measured upon THz self-mixing. Both measurements are in good agreement, thus ensuring a minimum amount of device

drift during the THz rectification experiments and adding to the credibility of the results. GFETs with top-gate configuration experience parasitic series resistances as a result of the ungated graphene regions. In our design, we maximized the channel transconductance – to which the rectified THz response is proportional, see Equation (1) below – by keeping the ungated channel regions small relative to the gated area.³³ Therefore, a gated channel region of length $L_g = 2.5 \mu\text{m}$ and a source-drain and drain-gate separation of 100 nm were chosen. The carrier mobility was extracted from the R_{DS} data³⁴ and the electron and hole mobilities were found to be $\mu_e \approx 1800 \text{ cm}^2/\text{Vs}$ and $\mu_h \approx 1200 \text{ cm}^2/\text{Vs}$, respectively. These relatively low mobilities are due to interactions with the substrate as well as impurities introduced during processing, with CVD graphene mobilities reported as much as one order of magnitude lower²⁹ than the best values reported for exfoliated graphene on SiO_2 .¹¹

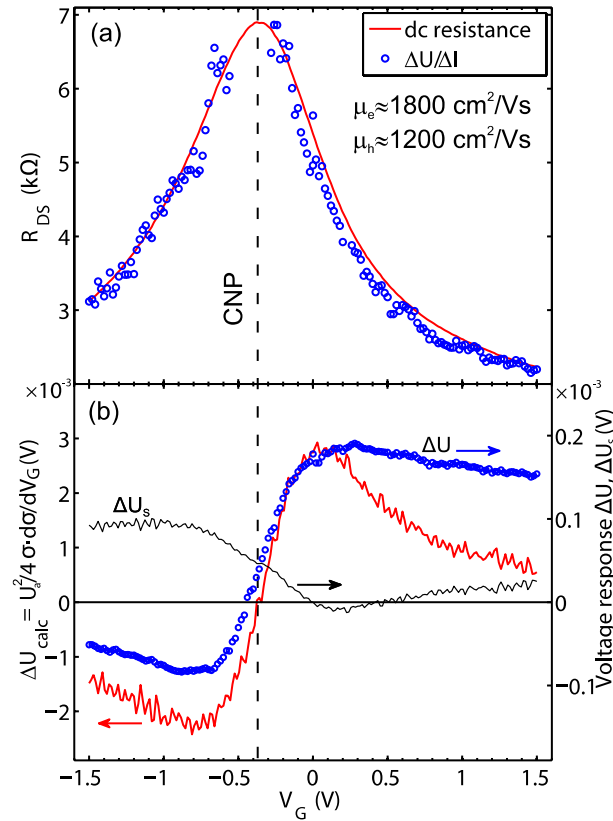


Figure 2. (a) Resistance of the GFET detector measured as dc resistance (red line) and as the ratio of the detected THz voltage and current response (symbols). (b) Anticipated rectified voltage ΔU_{calc} calculated from the dc resistance (red line) and measured voltage response ΔU at 0.6 THz (symbols). The thin black line shows the contribution ΔU_S of the thermoelectric effect. The dashed line displays the location of the charge neutrality point (CNP) from dc measurement.

The charge carrier transport and the THz rectification mechanisms in FETs can be described by hydrodynamic transport models when $\omega\tau \ll 1$,^{26,28} with the coupled radiation frequency ω and the scattering time $\tau \sim \mu m^*/e$. Here, $m^* = \hbar k_F/v_F$ is the effective cyclotron mass of the charge carriers and e is the electron charge.^{15,35} We assume the typical Fermi velocity in graphene $v_F \sim 10^6$ m/s and calculate the Fermi momentum $k_F = \sqrt{\pi n} \sim 2 \times 10^8$ m⁻¹ from the charge carrier density $n = \epsilon_r \epsilon_0 V_G / ed \sim 1.5 \times 10^{16}$ m⁻² with $\epsilon_r \sim 9$ and $d = 17$ nm for our design. The resulting charge carrier scattering time is $\tau \sim 25$ fs and with this we find that at our working frequency of 0.6 THz, $\omega\tau \sim 0.09$. Under such conditions, the transistor's channel can be modeled as a transmission line rather than a lumped element in the classical resistive mixing case, thus, this regime has been termed the *distributed resistive mixing regime*.^{27,36} Resonant detection cannot be expected in this regime because the excited plasma waves in the transistor are overdamped (enhanced plasmonic mixing requires $\omega\tau \gg 1$).²⁶ However, if the charge carrier mobility is increased, e.g., by selecting an alternate substrate³⁷ or suspending the graphene above the substrate,³⁸ graphene remains a promising candidate for the realization of resonant FET detectors.

In the non-resonant, distributed resistive mixing regime, where rectification occurs through self-mixing of overdamped radiation-induced charge density waves, the transistor channel's complex impedance can be simulated with transmission line models.²⁷ When designing FETs for

high frequency mixing, it must be taken into account that the real part of the impedance decreases with frequency and is substantially lower than in the quasi-stationary case of classical resistive mixing. Based on these considerations, we designed the integrated split bow-tie antennas (using commercial method-of-moments and time domain numerical electromagnetic solvers) and GFETs to ensure good matching conditions between the antenna impedance and the GFET channel impedance at 0.6 THz.

In Figure 2(b), the rectified 0.6 THz voltage response measured with a lock-in amplifier at a modulation frequency of 333 Hz with the setup shown in Figure 1(c) is plotted as open symbols on the right axis. The same figure shows as a red line on the left axis the theoretically expected optical voltage response of the detector at 0.6 THz (assuming a signal amplitude of $U_a = 1$ V), as calculated from the dc resistance data following Refs. 22 and 39 (Equation 1)

$$\Delta U_{calc} = \frac{U_a^2}{4\sigma} \frac{d\sigma}{dV_G},$$

where $\sigma = W/L/R_{DS}$ is the drain-source conductivity of the GFET (here, we neglect contact resistances). Because of the qualitative comparability of both curves one tends to presume that the rectification of the incident THz signal can be comprehensively described by distributed resistive mixing.³⁹ However, the measured response differs from the anticipated signal in two main aspects. First, the pronounced roll-off of the signal level at higher positive and negative gate bias voltages is hardly represented by the experimental curve. Second, at the charge neutrality point (CNP) at $V_G \sim -0.345$ V, it is expected that the rectified signal – proportional to the derivative of the channel conductivity – vanishes completely. The measured response, nevertheless, shows a significant magnitude at this point of ~ 49 μ V. A small leftward shift of the CNP, not precisely accessible in the resistance calculated from current and voltages responses due to divergence, could be partly responsible for this signal. However, such a shift is

indicated only for positive gate voltages by comparing the resistances in Figure 2(a). Accordingly, regarding these two features, it is highly likely that additional contributions to the classical Dyakonov-Shur THz response²⁶ are present in the detected signal and the simple model from Equation 1 does not give a comprehensive estimate of the response of the GFET detector.

We believe that one reason for the response offset at the CNP can be of thermophotovoltaic origin as has been proposed.²² By the asymmetric coupling of the THz radiation to the transistor channel feeds, energy is concentrated in the gated graphene region, close to one junction between the gated and ungated region, whereas the second junction is at the temperature of thermal equilibrium. We roughly estimate the generated thermoelectric voltage from the Seebeck coefficients in the gated and ungated regions S_g and S_{ug} , respectively. For graphene, the coefficients can be calculated from Mott's relation for degenerate semiconductors^{40,41} (Equation 2)

$$S = - \frac{\pi^2 k_B^2 T}{3e} \frac{1}{\sigma} \frac{d\sigma}{dV_G} \frac{dV_G}{dE} \Big|_{E=E_F},$$

with $E_F = \hbar k_{FVF}$. Assuming $S_{ug} = S_g(V_G = 0)$, at the CNP the thermoelectric voltage from the difference $\Delta U_S = S_g - S_{ug}$ gives $\sim 46.5 \mu\text{V/K}$. Hence, a temperature difference of roughly 1 K between the two junctions can be accountable for the additional contribution to the photoresponse at the CNP. A plot of the calculated thermoelectric voltage ΔU_S versus gate voltage is given in Figure 2(b) as a thin black line on the right axis. The main contribution of the effect is at negative gate voltages, yielding a possible explanation for the signal offset at these gate biases, in particular for the offset at the location of the CNP. In contrast, the different behaviour of the measured and calculated responses for higher positive gate voltages remains almost unchanged and cannot easily be explained by local heating effects. While these estimates

seem plausible for the particular experiment of this paper,^{41,42} clearly, further experimental and theoretical studies are required to verify the contribution of the thermoelectric effect to THz detection with GFETs. A full model would also have to account for carrier diffusion between the gated and ungated regions as well as modulations of the Fermi-level in the relatively short ungated regions due to fringing field effects.

From the measured responses, the voltage and current responsivity \mathfrak{R}_V and \mathfrak{R}_I , respectively, of the detector were calculated via (Equation 3)

$$\mathfrak{R}_V = \frac{\pi}{\sqrt{2}} \frac{\Delta U}{P} = R_{DS} \mathfrak{R}_I$$

and are shown in Figure 3(a). The prefactor $\pi/\sqrt{2} \approx 2.2$ originates from the Fourier transform of the square-wave modulated THz signal detected as rms value with a lock-in amplifier. This has an input impedance of 10 M Ω when measuring the voltage response. Furthermore, the GFET impedance is an order of magnitude higher than the lock-in amplifier input impedance when measuring the current response. The accuracy of both readout modes is ensured by the close overlap of the resistance curves in Figure 2(a) and also confirmed as the responses were independent of modulation frequency in the range 33 Hz – 33 kHz.³⁹ In the calculation of responsivity, the power P is taken as the total available beam power (29 μ W) measured after the collimating PTFE lens. Therefore, the presented responsivities are lower limits, as not all of the beam power was coupled to the GFET due to optical losses in the experimental system as well as impedance mismatching between the antenna and the GFET channel.

The sensitivity of the detector is calculated from the optical voltage responsivity \mathfrak{R}_V and the detector noise voltage V_N as (Equation 4)

$$NEP = \frac{V_N}{\mathfrak{R}_V} = \frac{\sqrt{4k_B T R_{DS}}}{\mathfrak{R}_V}.$$

Here, T is room temperature, and k_B is Boltzmann's constant. To support the use of thermal Johnson-Nyquist noise in Equation 4, the inset of Figure 3(b) shows measurements of the noise spectral density of a GFET detector comparable to the one used in the presented experiment – only differing in gate-width – at three different gate voltages. The dashed black lines represent the value of the thermal noise spectral density $4k_BTR_{DS}$ at the respective gate biases. Deviations from the measured noise levels are less than 15% and are due to charging of defect states altering the conductivity of the GFET channel. The minimum measured NEP for our detectors was 515 pW/Hz^{0.5}; the data are plotted in Figure 3(b). As with the responsivities, these values are a conservative estimate of the device NEP, not taking into account any coupling losses of the THz radiation to the GFET channel. Nonetheless, the values are a substantial improvement over the best reported performance of antenna-coupled single-layer exfoliated GFET detectors.²²

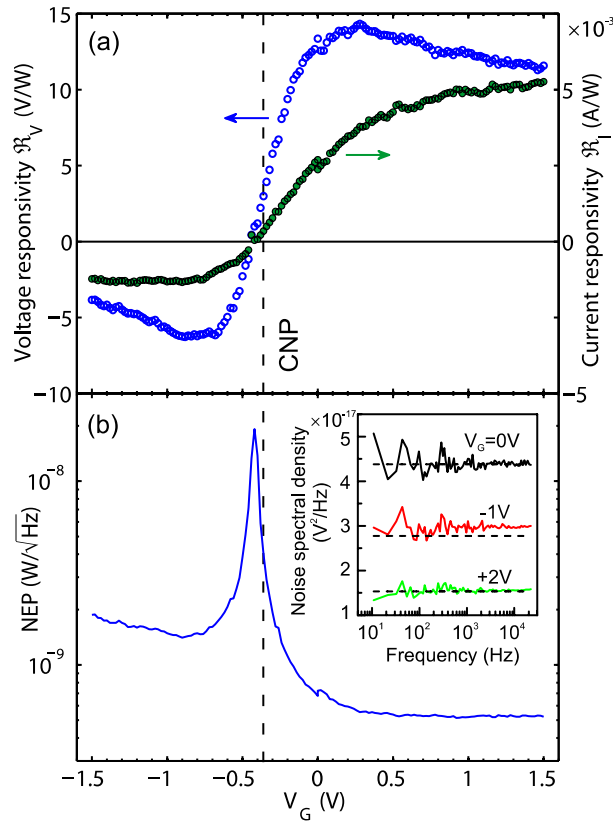


Figure 3. (a) Voltage (open symbols) and current (closed symbols) responsivity of the GFET detector at 0.6 THz. (b) NEP of the detector calculated from the voltage responsivity. The minimum measured NEP was 515 pW/Hz^{0.5}. The inset shows the measured noise spectral density at different gate biases of a representative GFET detector with 5 μm gate width. The black dashed lines represent the calculated thermal noise at the respective gate biases.

This considerable improvement in NEP is ultimately a result of the enhanced responsivity, originating from a careful antenna design and using a top-gated device design while minimizing the contact resistances. The relationship of Equation (1) may be written in terms of the ability to alter the current with the gate voltage, i.e. $\Delta U \propto \frac{dI_{DS}}{dV_G}$. Consequently, our detectors directly benefit from the top-gate configuration by a higher gate capacitance per area, $C_{ox} = \epsilon_{ox}/t_{ox}$, compared to a SiO₂ back-gate.²³ Furthermore, the major improvement in NEP when comparing to Refs. 21 and 22, with similar C_{ox} , results from the drastically reduced ungated regions; known to seriously deteriorate the on-off ratio in GFETs due to large contact resistances.^{14,34}

In conclusion, we have for the first time successfully demonstrated room-temperature detection at 0.6 THz with highly sensitive CVD-grown graphene FET detectors with integrated split bow-tie antennas. Proper device design allowed an efficient channel modulation and reduced parasitic capacitances. Together with an optimized antenna, this results in a major improvement of the voltage responsivity and NEP over previous studies in both single-layer and bilayer graphene.^{21,22} For our detectors, we find a minimum NEP of 515 pW/Hz^{0.5}. Further investigation is necessary to determine the physical processes occurring in the GFET channel under THz illumination in addition to the classical Dyakonov-Shur detection mechanism. While models describing the distributed resistive mixing mechanism have been developed for semiconductor FET detectors²⁷ and ideal graphene sheets,¹⁵ none has been shown for graphene of our

experimental quality. The apparent shift in responsivity (asymmetry or equivalently offset of responsivity around the Dirac voltage) has not been observed for other detector technologies, but have been reported before for graphene FET detectors.^{21,22} This suggests that previously-developed models are not sufficient to comprehensively describe THz detection in graphene-based FETs. In this context, the contribution of thermoelectric effects to the measured rectified THz signals was discussed. Finally, we demonstrated that CVD graphene-based FET detectors show their potential to compete with other detector technologies, which opens the possibility for scalable graphene-detector production.

AUTHOR INFORMATION

Corresponding Author

*E-mail: andmic@chalmers.se *E-mail: audreyz@student.chalmers.se, *E-mail:
m.bauer@physik.uni-frankfurt.de.

Author Contributions

M.A. A., A. Z. and M. B. designed and fabricated the devices. M.A. A., A. Z., M. B. and A. L. performed the electrical and optical characterization. J. M. and A. L. are responsible for the noise measurements. M.A. A., A. Z. and M. B. equally contributed to the writing of the manuscript. All authors contributed to discussions and the analysis and interpretation of the results. All authors have given approval to the final version of the manuscript.

Notes

The authors declare no competing financial interest.

ACKNOWLEDGMENT

This work was supported by the Swedish Foundation of Strategic Research (SSF), Knut and Alice Wallenberg Foundation (KAW) the Swedish Research Council Project 2012-4978. The Frankfurt team acknowledges support by the Hessian excellence initiative LOEWE "Sensors towards Terahertz". A.L. and J.M. are thankful for funding by the European Social Fund under the Global Grant measure.

REFERENCES

- (1) Appleby, R.; Wallace, H.B. *IEEE Trans. Antennas Propag.* **2007**, *55*, 2944-2956.
- (2) Federici, J.F.; Schulkin, B.; Huang, F.; Gary, D.; Barat, R.; Oliveira, F.; Zimdars, D. *Semicond. Sci. Technol.* **2005**, *20*, S266-S280.
- (3) Siegel, P.H. *IEEE Trans. Microwave Theory Tech.* **2004**, *52*, 2438-2447.
- (4) Öhrström, L.; Bitzer, A.; Walther, M.; Ruehli, F.J. *Am. J. Phys. Anthropol.* **2010**, *142*, 497-500.
- (5) Tonouchi, M. *Nat. Photonics.* **2007**, *1*, 97-105.
- (6) Knap, W.; Dyakonov, M.; Coquillat, D.; Teppe, F.; Dyakonova, N.; Lusakowski, J.; Karpierz, K.; Sakowicz, M.; Valusis, G.; Seliuta, D. *J. Infrared Millim. Terahertz Waves*, **2009**, *30*, 1319-1337.
- (7) Sherry, H.; Al Hadi, R.; Grzyb, J.; Öjefors, E.; Cathelin, A.; Kaiser, A.; Pfeiffer, U.R. Lens-integrated THz imaging in 65nm CMOS technologies. In *Radio Frequency Integrated Circuits Symposium (RFIC), 2011 IEEE*. June 5-7, 2011, 1-4.

- (8) Bauer, M.; Venckevičius, R.; Kašalynas, I.; Boppel, S.; Mundt, M.; Minkevičius, L.; Lisauaskas, A.; Valušis, G.; Krozer, V.; Roskos, H.G. *Opt. Express*, in press.
- (9) Sun, J.D.; Sun, Y.F.; Wu, D.M.; Cai, Y.; Qin, H.; Zhang, B.S. *Appl. Phys. Lett.* **2012**, *100*, 013506.
- (10) Bauer, M.; Lisauskas, A.; Boppel, S.; Mundt, M.; Krozer, V.; Roskos, H.G.; Chevtchenko, S.; Wuerfl, J.; Heinrich, W.; Traenkle, G. Bow-tie-antenna-coupled terahertz detectors using AlGaIn/GaN field-effect transistors with 0.25 micrometer gate length. In *2013 8th European Microwave Integrated Circuits Conference (EUMIC) (2013) 212-215*, 8th European Microwave Integrated Circuits Conference (EuMIC), Nuremburg, Germany, Oct. 6-8, 2013.
- (11) Novoselov, K.S.; Geim, A.K.; Morozov, S.V.; Jiang, D.; Zhang, Y.; Dubonos, S.V.; Grigorieva, I.V.; Firsov, A.A. *Science* **2004**, *306*, 666-669.
- (12) Castro Neto, A.H.; Guinea, F.; Peres, N.M.R.; Novoselov, K.S.; Geim, A.K. *Rev. Mod. Phys.* **2009**, *81*, 109-162.
- (13) Otsuji, T.; Tombet, S.A.B.; Satou, A.; Fukidome, H.; Suemitsu, M.; Sano, E.; Popv, V.; Ryzhii, M.; Ryzhii, V. *MRS Bull.* **2012**, *37*, 1235-1243.
- (14) Schwierz, F. *Proc. IEEE* **2013**, *101*, 1567-1584.
- (15) Tomadin, A.; Polini, M. *Phys. Rev. B* **2013**, *88*, 205426.
- (16) Tomadin, A.; Tredicucci, A.; Pellegrini, V.; Vitiello, M.S.; Polini, M. *Appl. Phys. Lett.* **2013**, *103*, 211120.

- (17) Wu, Y.; Jenkins, K.A.; Valdes-Garcia, A.; Farmer, D.B.; Zhu, Y.; Bol, A.A.; Dimitrakopoulos, C.; Zhu, W.; Xia, F.; Avouris, P.; Lin, Y.-M. *Nano Lett.* **2012**, *12*, 3062-3067.
- (18) Moon, J.S.; Seo, H.-C.; Antcliffe, M.; Lin, S.; McGuire, C.; Le, D.; Nyakiti, L.O.; Gaskill, D.K.; Campbell, P.M.; Lee, K.-M.; Asbeck, P. *IEEE Electron Device Lett.* **2012**, *33*, 1357-1359.
- (19) Guo, Z.; Dong, R.; Chakraborty, R.S.; Lourenco, N.; Palmer, J.; Hu, Y.; Ruan, M.; Hankinson, J.; Kunc, J.; Cressler, J.D.; Berger, C.; de Heer, W.A. *Nano Lett.* **2013**, *13*, 942-947.
- (20) Habibpour, O.; Vukusic, J.; Stake, J. *IEEE Trans. Microwave Theory Tech.* **2013**, *61*, 841-847.
- (21) Spirito, D.; Coquillat, D.; De Bonis, S.L.; Lombardo, A.; Bruna, M.; Ferrari, A.C.; Pellegrini, V.; Tredicucci, A.; Knap, W.; Vitiello, M.S. *Appl. Phys. Lett.* **2014**, *104*, 061111.
- (22) Vicarelli, L.; Vitiello, M.S.; Coquillat, D.; Lombardo, A.; Ferrari, A.C.; Knap, W.; Polini, M.; Pellegrini, V.; Tredicucci, A. *Nat. Mater.* **2012**, *11*, 865-871.
- (23) Muraviev, A.V.; Rumyantsev, S.L.; Liu, G.; Balandin, A.A.; Knap, W.; Shur, M.S. *Appl. Phys. Lett.* **2013**, *103*, 181114.
- (24) Bevilacqua, S.; Cherednichenko, S. Fast room temperature THz bolometers. *Proceedings of the 38th International Conference on Infrared, Millimeter, and Terahertz Waves (IRMMW-THz)*, Mainz, Germany, Sept. 1-6, 2013.
- (25) Liu, L.; Hesler, J.L.; Xu, H.; Lichtenberger, A.W.; Weikle, II, R.M. *IEEE Microwave Wireless Compon. Lett.* **2010**, *9*, 504-506.
- (26) Dyakonov, M.; Shur, M. *IEEE Trans. Electron Devices* **1996**, *43*, 380-387.

- (27) Boppel, S.; Lisauskas, A.; Mundt, M.; Seliuta, D.; Minkevičius, L.; Kašalynas, I.; Valušis, G.; Mittendorf, M.; Winnerl, S.; Krozer, V.; Roskos, H.G. *IEEE Trans. Microwave Theory Tech.* **2012**, *60*, 3834-3843.
- (28) Dyakonov, M.; Shur, M. *Phys. Rev. Lett.* **1993**, *71*, 2465-2468.
- (29) Sun, J.; Lindvall, N.; Cole, M.T.; Angel, K.T.T.; Wang, T.; Teo, K.B.K.; Chua, D.H.C.; Liu, J.; Yurgens, A. *IEEE Trans. Nanotechnol.* **2012**, *11*, 255-260.
- (30) de la Rosa, C.J.L.; Sun, J.; Lindvall, N.; Cole, M.T.; Nam, Y.; Löffler, M.; Olsson, E.; Teo, K.B.K.; Yurgens, A. *Appl. Phys. Lett.* **2013**, *102*, 022101.
- (31) Kim, S.; Nah, J.; Jo, I.; Shahrjerdi, D.; Colombo, L.; Yao, Z.; Tutuc, E.; Banerjee, S.K. *Appl. Phys. Lett.* **2009**, *94*, 062107.
- (32) Wang, H.; Wu, Y.; Cong, C.; Shang, J.; Yu, T. *ACS Nano* **2010**, *4*, 7221-7228.
- (33) Tanzid, M.; Andersson, M.A.; Sun, J.; Stake, J. *Appl. Phys. Lett.* **2014**, *104*, 013502.
- (34) Habibpour, O.; Vukusic, J.; Stake, J. *IEEE Trans. Electron Devices* **2012**, *59*, 968-975.
- (35) Ryzhii, V. *Jpn. J. Appl. Phys.* **2006**, *45*, L923.
- (36) Lisauskas, A.; Pfeiffer, U.; Öjefors, E.; Bolivar, P.H.; Glaab, D.; Roskos, H.G. *J. Appl. Phys.* **2009**, *105*, 114511.
- (37) Dean, C.R.; Young, A.F.; Meric, I.; Lee, C.; Wang, L.; Sorgenfrei, S.; Watanabe, K.; Taniguchi, T.; Kim, P.; Shepard, K.L.; Hone, J. *Nat. Nanotechnol.* **2010**, *5*, 722-726.

(38) Bolotin, K.I.; Sikes, K.J.; Hone, J.; Stormer, H.L.; Kim, P. *Phys. Rev. Lett.* **2008**, *101*, 096802.

(39) Sakowicz, M.; Lifshits, M.B.; Klimenko, O.A.; Schuster, F.; Coquillat, D.; Teppe, F.; Knap, W. *J. Appl. Phys.* **2011**, *110*, 054512.

(40) Cutler, M.; Mott, N.F. *Phys. Rev.* **1969**, *181*, 1336.

(41) Xu, X.; Gabor, N.M.; Alden, J.S.; van der Zande, A.M.; McEuen, P.L. *Nano Lett.* **2010**, *10*, 562-566.

(42) Zuev, Y.; Chang, W.; Kim, P. *Phys. Rev. Lett.* **2009**, *102*, 096807.

TABLE OF CONTENTS GRAPHICS

